Available online at www.sciencedirect.com
ScienceDirect
Chemical Physics Letters 447 (2007) 221–226
CHEMICAL PHYSICS LETTERS
www.elsevier.com/locate/cplett

Real-time vibrational amplitude change in the ground and excited states of a quinoid thiophene induced by few-cycle pulses

Zhuan Wang [a,b], Takayoshi Kobayashi [a,b,c,d,*]

[a] Department of Applied Physics and Chemistry and Insititute of Laser Science, University of Electro-communications, Chofugaoka 1-5-1, Chofu, Tokyo 182-8585, Japan
[b] JST, ICORP, Ultrashort Pulse Laser Project, 4-1-8 Honcho, Kawaguchi, Saitama, Japan
[c] Department of Electrophysics, National Chiao Tung University, 1001 Ta Hsueh Road Hsinchu 300, Taiwan
[d] Institute of Laser Engineering, Osaka University, Yamadakami 2-6, Suita 565-0871, Ibaraki 567-0047, Japan

Received 9 July 2007; in final form 31 August 2007
Available online 7 September 2007

Abstract

Several vibrational modes impulsively excited by 6.7 fs pulses were observed in a quinoid thiophene. From the amplitude decay time and the phase of vibration, the modulation mechanism of the electronic transition by the wave packet motion is discussed and classified in terms of vibronic coupling. Modes with wavenumbers of 1343 and 1420 cm^{-1} are attributed to the wave packet motions on the potential surface of the excited and ground state, respectively, and a mode with 1539 cm^{-1} is due to those of both states. The apparent low-frequency modulation of these three modes is ascribed to the artificial interference effect in the calculation of the spectrogram.

1. Introduction

The real-time observation of molecular vibration dynamics has been realized by utilizing an impulsive excitation with femtosecond lasers [1–6]. Coherent vibrational modes of molecules are well formulated by time-dependent nuclear wave packet description, by which one may be able to set theoretical bases of models of chemical reaction pathways and geometrical changes associated with the electronic excitations using the experimental results and even predict novel phenomena. In particular, the wave packet dynamics in the excited states of molecules is important for coherent control of molecular systems [1–6]. A pump–probe experiment with resonant femtosecond pulses to the electronic transition can be used to observe the wave packet dynamics on the surfaces of the relevant excited state or the ground state. The detectable vibrational frequency has an upper bound limited by the pulse duration and the step time of the pump–probe decay. It has also a lower bound limited by the measurement time span of the delay and the lifetimes of the excited species or intermediates of interest.

In spite of extensive studies of coherent control and coherent molecular vibrational modes, the mechanism of induced coherent molecular vibration has not yet been well understood. In this Letter, we have studied the origin of the signals appearing in a modulation of electronic transition and assigned it to the motion of the wave packet in either the ground- or excited-state potential surface.

A novel quinoid thiophene was selected as a sample because the *s-trans–cis*-configuration is a good prototype of polyacetylene [7,8], which is of interest from the viewpoint of vibronic coupling and non-linear reactions such as solitons, polarons and breathers [9]. This is quite different from that of the thiophene oligomer with an aromatic structure containing both *s-trans* and *s-cis* configurations with a nearly equal amount.

* Corresponding author. Address: Department of Applied Physics and Chemistry and Insititute of Laser Science, University of Electro-communications, Chofugaoka 1-5-1, Chofu, Tokyo 182-8585, Japan. Fax: +81 42 443 5825.
E-mail addresses: wang@ils.uec.ac.jp (Z. Wang), kobayashi@ils.uec.ac.jp (T. Kobayashi).

0009-2614/$ - see front matter © 2007 Elsevier B.V. All rights reserved.
doi:10.1016/j.cplett.2007.08.094

2. Experimental

The concentration of tetrahydrofuran (THF) solution of QT2 was 1.5×10^{-4} mol/dm^3. The structure of the molecule is shown in the inset of Fig. 1. In the present study, the sample in the THF solution in a 1 mm quartz cell has an optical density of 1.6 at the absorption peak at 690 nm. The stationary absorption and the fluorescence spectra of QT2 were recorded with an absorption spectrometer (Shimadzu, UV-3101PC) and a fluorophotometer (Hitachi, F-4500), respectively.

Femtosecond time-resolved pump–probe spectroscopy was performed with an experimental setup described in Refs. [10–12]. Important parameters of the experimental system are as follows: The 5 kHz chirp compensated pulse train from a non-collinear optical parametric amplifier [13–15] was split into two beams for pump–probe spectroscopy. The energy and the intensity of the pump pulse at the sample were ~40 nJ and 0.18 GW/cm^2, respectively. The pump–probe signals were detected with a multi-channel lock-in amplifier. Real-time spectra were taken at delay times from ~−200 to 2000 fs with 1 fs step. All the experiment was performed at room temperature (293 ± 1 K).

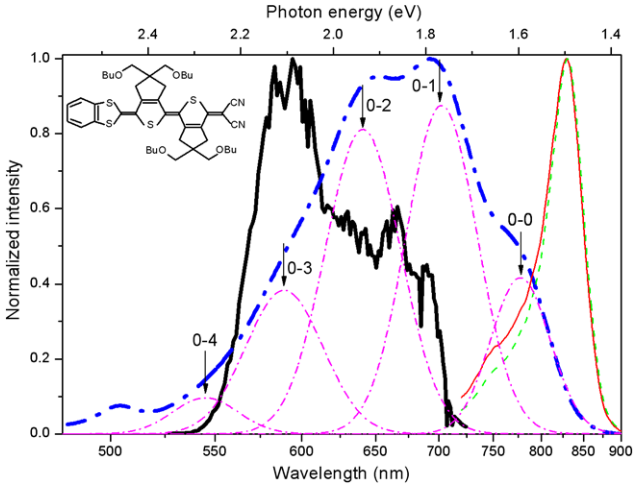

Fig. 1. Spectra of laser output (thick solid line), stationary absorption (dash-dotted line), spontaneous fluorescence (thin solid line) and stimulated emission (dashed line) calculated from the spontaneous fluorescence spectrum. The curves in dashed line are the results of the simulation of the Huang–Rhys factor. The inset is the structure of the molecule used in the present study.

3. Results and discussion

3.1. Stationary absorption and fluorescence spectra and electronic decay dynamics

Fig. 1 shows the absorption, fluorescence, and laser spectra. The absorption spectrum has peaks at 650 and 690 nm and a shoulder at 760 nm. This feature can be explained in terms of the vibronic structure of a mode having the wavenumber of 1370 cm^{-1} with the Huang–Rhys factor of 1.69.

Fig. 2 shows the real-time traces of the difference absorbance probed in the range between 535 and 590 nm. By

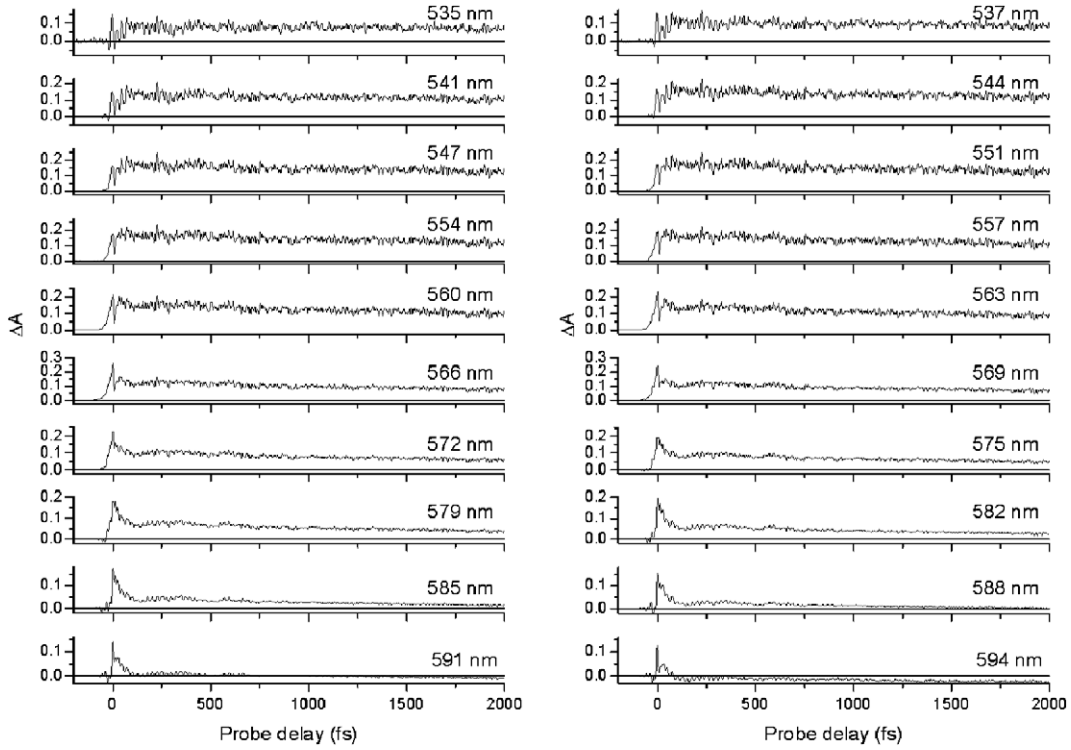

Fig. 2. Real-time traces of the difference absorbance probed at different wavelengths in the spectral range between 535 and 595 nm.

shifted averaging to remove the effect of vibration, the pure electronic decay and/or growth dynamics were analyzed to be composed of two states with lifetimes of 50 ± 5 fs and slightly longer than 2 ps. There are three possible candidates of the shorter component. It can be (1) the transition ($S_m \leftarrow S_1$, $m \geqslant 2$) from the lowest excited state (S_1) to a higher excited state (S_m), (2) the transition ($S_m \leftarrow S_n$, $m > n \geqslant 2$) from a higher excited singlet state $S_n (n \geqslant 2)$ to a still higher state (S_m), and (3) the transition ($S_m \leftarrow S_1^*$) from a hot vibrational state in the lowest excited state (S_1^*). In these cases the candidates of long-life components are (1) the triplet state, (2) the lowest excited state (S_1), and (3) vibrationally relaxed electronic excited states (S_1). The candidate (1) can be ruled out because the lifetime is estimated to be too short to be the relaxed electronic state, S_1, from the relatively intense fluorescence. The fluorescence originates from an equilibrium state, and the yield is roughly estimated to be 0.01. From the ground-state absorption spectrum, the natural lifetime is estimated to be of the order of 10 ns. Therefore, the lifetime of the thermal equilibrium S_1, ~100 ps, is several orders of magnitude longer than 50 fs. From the slopes of the real-time traces, the upper limit of this lifetime is estimated to be 10 ps. The candidate (2) can also be eliminated for the following reason: In the pump wavelength region, there are no indications of strongly absorbing electronic state other than the ($S_1 \leftarrow S_0$) transition, which can be well filled with the Huang–Rhys factor of 1.69, as described earlier; see Fig. 1. Since the wavelength-dependent bleaching spectrum observed in the region from 535 to 600 nm is expected to be proportional to the ground-state absorption, it is difficult to attribute it to the much weaker absorption, if any, hidden in the strong $S_1 \leftarrow S_0$ absorption. Therefore, the component with a lifetime of 50 fs is assigned to the hot lowest electronic excited state (S_1^*).

The above discussion is based on the assignment of 50 fs to the electronic relaxation. There is yet another possibility of the observed dynamics, i.e., a change induced by the breather mode discussed in Ref. [17]. In our study of nanopolyacetylene [17], we found experimentally for the first time that the C–C stretching modes were modulated with the breather mode just after excitation [17–26]. In this case, the breather is confined in a limited size of QT2 molecule and can exist for more than 2 ps as in a confined 'soliton pair', like the exciton found in polyphenylacetylene [27–29].

In the range of 535–590 nm, the contribution of the excited-state absorption to the transient spectra is more intense than those of bleaching and induced emission with a negative ΔA signal. In the present Letter, we concentrate on the molecular vibrational dynamics coupled to the electronic spectrum in this region.

3.2. Classification of the wave packet motion

Fourier transform (FT) was performed with cosine functions after subtraction of the slow dynamics of electronic relaxation from the traces. They show more than twenty vibrational modes appearing as a modulation of the transition possibility. Among them, 12 vibrational modes with higher intensities were studied in our previous paper in terms of the wavelength dependence of their phases and amplitudes around 97, 142, 301, 525, 785, 1172, 1343, 1376, 1420, 1453, 1510, and 1539 cm^{-1} [16].

Table 1
Wavenumbers, phases and wavelength ranges of the modes appearing in the FT of the real-time trace and wave packet classification

Modes (cm^{-1})	Phase (π)	Wavelength range (nm)	Wave packet contribution (%)	
			Ground state	Excited state
97	(−0.7 ~0.3)	540–570	–	–
	~0.20	570–590	24	66
142	~0.89	540–590	~11	~89
301	~−0.11	540–590	~11	~89
525	~0.11	540–590	~11	~89
785	~−0.05	540–590	~2	~98
1172	~0.53	540–590	~99	~1
1343	~0.16	540–590	~23	~77
1376	~−0.89	540–590	~11	~89
1420	~−0.52	540–590	~99	~1
1453	~0.13	540–590	~16	~84
1510	~−0.51	540–590	~100	~0
1539	~−0.33	540–590	~74	~26

Table 1 shows results of the classification of wave packet motions. The modes of wavenumbers with 97, 142, 301, 525, and 785 cm^{-1} are mainly assigned to the excited-state wave packets by the fact that the phases of the molecular vibrational modes are close to 0π or $\pm\pi$ [30,31]. The modes of 1172, 1420, and 1510 cm^{-1} are mainly assigned to the ground-state wave packets impulsively generated by the stimulated Raman process within the pump pulse duration because their phases are close to $\pm(1/2)\pi$. All others seem to have contributions from both the ground- and excited-state wave packets.

The vibronic coupling mechanism was discussed in terms of the Condon and non-Condon types [10]. The former (modes 97, 301, 1172, 1343, 1420, and 1450 cm^{-1}) was divided into three subgroups characterized by the spectral change in shifting, breathing, and their mixed effects [16]. The latter could be classified into four subgroups: a change in the spectral intensity and the remaining three as mentioned above [16].

3.3. Time and wavelength dependence of vibrational amplitudes

Further analysis was performed to calculate the delay time dependence of the vibrational amplitudes via the spectrogram. The two-dimensional results are shown in Fig. 3. We find from Fig. 3b and c that they resemble each other in their distribution patterns of the high-amplitude range, which extends to longer delay time up to ~2 ps with their peaks around 550 nm. In contrast, Fig. 3a differs from

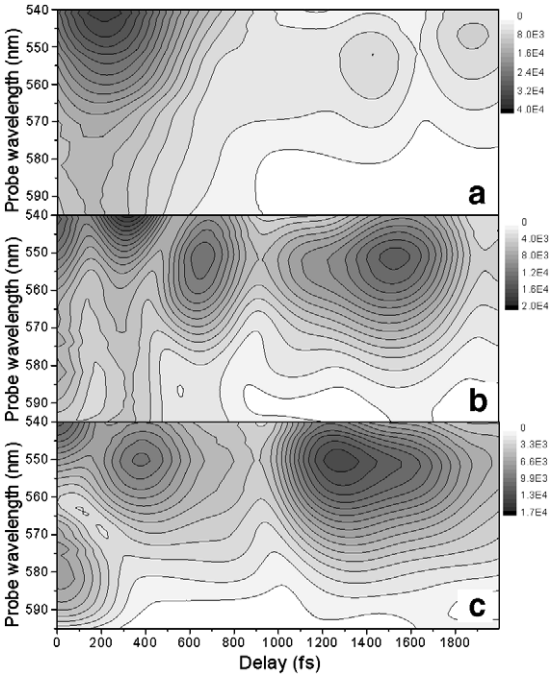

Fig. 3. Probe time and wavelength dependence of the vibrational amplitude calculated by spectrogram by use of the Blackman window of 500 fs FWHM, (a) 1343, (b) 1420, and (c) 1539 cm^{-1}.

the other two, showing a very high peak at 540 nm, which decays in a very short time.

To investigate the dynamics of the typical vibrational modes coupled to the ground state and/or excited state, the probe delay time (t) dependence of the vibrational amplitudes $A(t)$ for mode 1343 cm^{-1} are plotted in Fig. 4a, which could be fitted with a function of

$$A(t) = A_0 + A_1 e^{-t/\tau} \quad (1)$$

except for the oscillation. The terms A_0 corresponds to the signal with a lifetime much longer than 3 ps and A_1 to that with lifetime τ. The best-fit curve shown in Fig. 4a was obtained when $A_0 = 0.1 \pm 0.05$, $A_1 = 2.1 \pm 0.05$, and $\tau = 330 \pm 5$ fs. The fitting result indicates that the excited vibration disappears within 500 fs. It is hard to detect a molecular vibrational mode with such a short lifetime, because a very broad spectrum expected in a stationary Raman spectrum reduces the Raman peak intensity despite a relatively high frequency-integrated intensity (area), and the Raman signal may be smeared out into a very broad fluorescence spectrum. The lifetime of the parameter A_0 is estimated to be longer than 3 ps, because it does not decay at a delay time of 2 ps but even increases slightly. Therefore, the major fraction (~95%) represented by A_0 of the mode of the intensity modulation with 1343 cm^{-1} of the transition can definitely be attributed to the wave packet in the excited state. This finding agrees with those of the FT analysis of the real-time trace that the phase of the 1343 cm^{-1} mode is $\sim 0.16\pi$, which means that the wave packet motion is mainly from the excited state (~77%). The difference in the amount of contribution calculated from the decay analysis of the amplitude $A(t)$ and the phase is probably due mainly to the error in the estimation of the phase.

In Fig. 4b, the two curves for the 1420 and 1539 cm^{-1} modes show similar dynamics. Neither of them decays in the probed range of the decay time; they oscillate and the center amplitude of the oscillation even increases slightly. The FT analysis indicates that the 1420 cm^{-1} mode, with a phase of $\sim -0.52\pi$, is dominantly due to the ground-state wave packet and that the 1539 cm^{-1} mode with a $\sim -0.33\pi$ phase is due to the wave packet motion with 1/4 and 3/4 contributions from the excited- and ground-states, respectively.

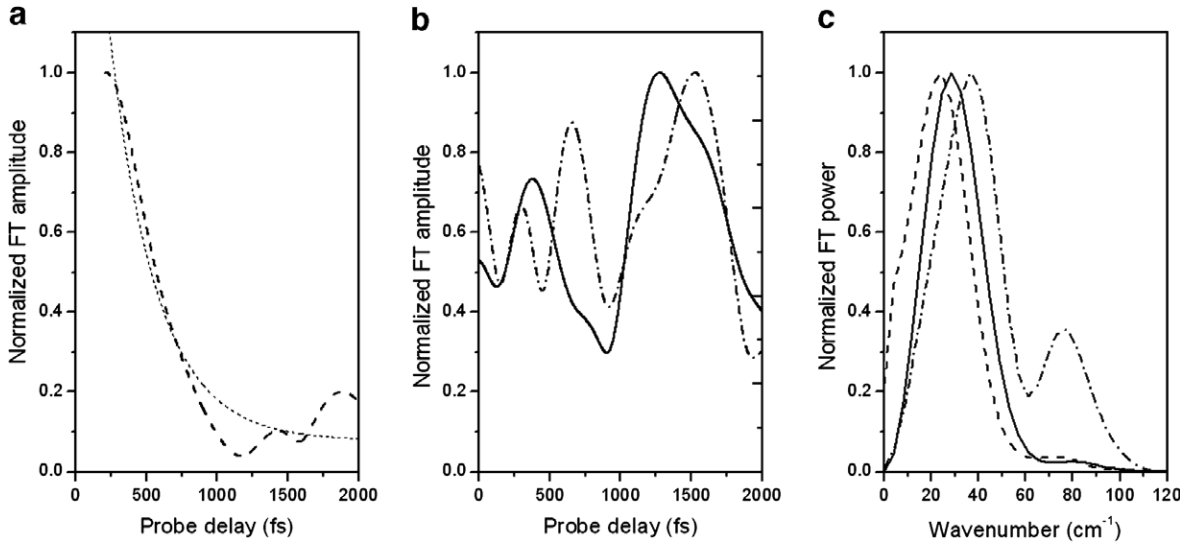

Fig. 4. (a) Probe delay dependent vibrational amplitude of mode 1343 cm^{-1} (dashed line) and the exponential fitting (thin dashed line); (b) probe delay dependent vibration amplitude of mode 1420 (dash-dotted line) and 1539 (solid line) cm^{-1}; (c) FT power spectra of the time dependent traces of the amplitudes shown in (a) and (b) of modes of 1343, 1420, and 1539 cm^{-1} in dashed, dashed-dotted, and solid line, respectively.

A probable reason for the absence of a rapid decay amplitude in the excited state is the width of the Blackman window that smears the contribution of the short lifetime component; as estimated from this disappearance, it can be shorter than 300 fs.

3.4. Interference among vibrational modes

The FT results of the curves in Fig. 4a and b are plot in Fig. 4c. The amplitude of the 1343 cm^{-1} mode has modulation wavenumbers of 24 and 77 cm^{-1} corresponding to the period of 1400 and 430 fs. The amplitude modulations for the 1420 cm^{-1} mode are 36 and 77 cm^{-1} corresponding to the periods of 920 and 430 fs. The modulation wavenumbers for 1539 cm^{-1} are 28 and 77 cm^{-1}, respectively and the corresponding periods are 1170 and 430 fs. These modulation wavenumbers are very close to the difference between some of the two neighboring vibrational modes appearing in the experiments: e.g., 77 cm^{-1} vs. the difference of 1420–1343 cm^{-1} and 36 cm^{-1} vs. 1457–1420 cm^{-1}. The origin of the modulation appearing in the vibrational frequency oscillation is explicable in the following way.

In a spectrogram analysis, there is a possibility of an artificial interference concerned with the narrow gate width used in the calculation process. To show this, the results of our simulation are shown in Fig. 5. The simulated trace is a linear combination of two functions,

$$A_i(t) = c_i \exp(t/\tau_i)\cos(\omega_i t), (i = 1, 2). \quad (2)$$

Here, ω_1 and ω_2 are the angular frequencies corresponding to the wavenumbers of 1420 and 1343 cm^{-1}, which have a difference of 77 cm^{-1}. In the simulation process, the FWHM of Blackman gate function is changed from 300 to 800 fs. As shown in Fig. 5, an amplitude modulation with a period of 420 fs corresponding to 80 cm^{-1} appears when the FWHM of the gate is narrower than 800 fs. This value is nearly equal to 77 cm^{-1}, and the difference between them arises from the experimental and/or calculation error. On the other hand, this interference nearly disappears when the FWHM of the gate window reaches 800 fs (~2 times the period of the mode difference of 77 cm^{-1}). However, the results shown in Fig. 3 are calculated with a 500 fs FWHM gate function, which is shorter than twice the corresponding periods of the modes of 24, 28, 36, and 77 cm^{-1}. So the following general features can be clarified.

According to the above simulation, the modulations of 24, 28, 36, and 77 cm^{-1} are due to the interferences in the analysis, and the fact that all these modes are missing in the experimental results also supports the above-mentioned finding. This is totally different from the case in polydiacetylene reported in Refs. [30,31]. In this case, the modulations of the amplitudes and wavenumbers of the C–C (1220 cm^{-1}) and C=C (1455 cm^{-1}) stretching modes are introduced from the C=C–C (230 cm^{-1}) bending mode, which appears in the FT power spectra of the real-time trace of the molecular vibrational amplitudes. The present results of simulation indicate that adequate attention should be given to the artificial interference affecting the analysis of mode coupling.

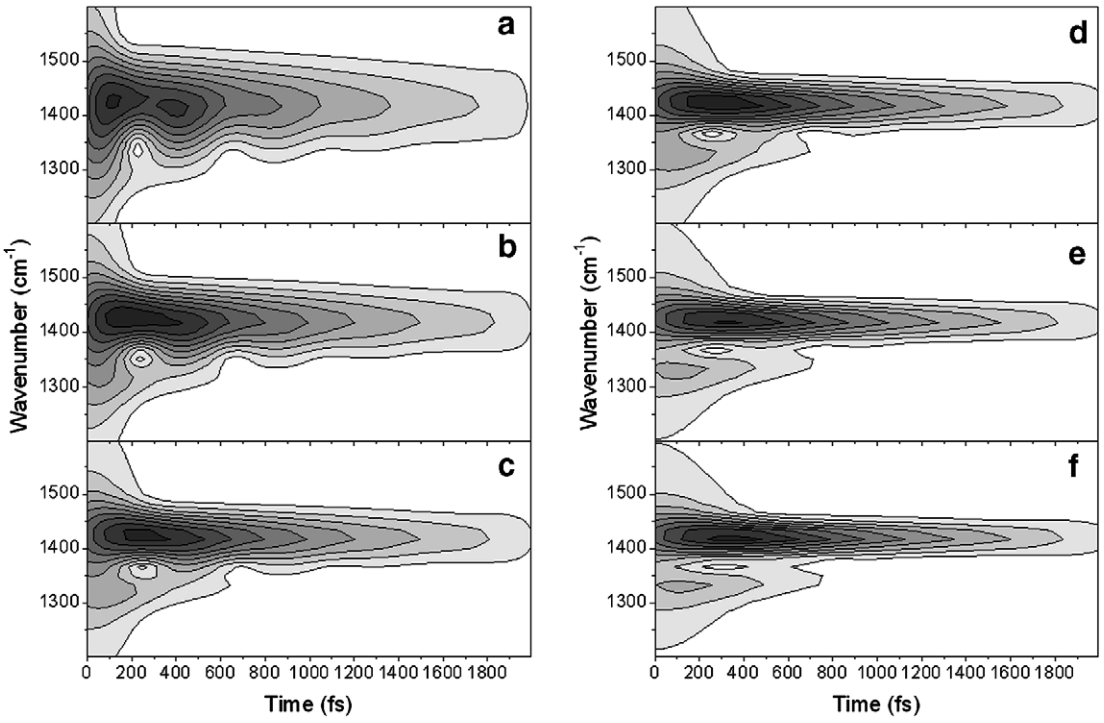

Fig. 5. Spectrograms of simulated traces with a linear combination of $A_1(t) = 1 * \exp(-t/\tau_1)\cos(\omega_1 t)$ and $A_2(t) = 0.5 * \exp(-t/\tau_2)\cos(\omega_2 t)$, where $\tau_1 = 1000$ fs and $\tau_2 = 333$ fs. (a–f) Spectrograms with Blackman gating windows of 300, 400, 500, 600, 700, and 800 fs FWHM, respectively.

4. Conclusion

With the aid of few-cycle pulses generated from the NOPA developed in our group, we have observed modulations of the vibrational amplitudes of several modulations impulsively excited in a quinoid thiophene within 2 ps. The origin of the vibrational signal appearing in the experimental results is studied in terms of the modulation of the electronic transition due to the wave packet motions. Modes of 1343 and 1420 cm^{-1} are mainly ascribed to the wave packet motions in the excited and ground states, respectively, and that of 1539 cm^{-1} to the combination of the two. The interference among the neighboring vibrational modes is discussed in terms of the analytical artifact. These apparent low-frequency modulations of the three modes are ascribed to the artificial interference effect in the calculation of the spectrogram. In the process of spectrogram calculation, the results are strongly affected by the gate window width at FWHM. It seems important to use a gate function with a window width (FWHM) of twice the corresponding period of the mode difference of the neighboring modes.

Acknowledgements

The authors are grateful to Prof. Emeritus Tetsuo Otsubo of Hiroshima University for providing us with the quinoid thiophene derivative QT2. This work was partly supported by the Grant MOE ATU Program in NCTU.

References

[1] A. Laubereau, M. Stockburger, Time-Resolved Vibrational Spectroscopy, Springer Verlag, Berlin, 1985.
[2] E. Schreiber, Springer Tracts in Modern Physics 143: Femtosecond Real-Time Spectroscopy of Small Molecules and Clusters, Springer, Berlin, 1998.
[3] F.C. De Schryver, S. De Feyter, G. Schwertzer, Femtochemistry, Wiley VCH, New York, 2001.
[4] M.M. Martin, J.T. Hynes, Femtochemistry and Femtobiology Ultrafast Events in Molecular Science, Elsevier, Amsterdam, 2004.
[5] P. Hannaford, Femtosecond Laser Spectroscopy, Springer, Berlin, 2005.
[6] A.W. Castleman Jr., M.L. Kimble, Femtochemistry VII Fundamental Ultrafast Processes in Chemistry Physics and Biology, Elsevier, Amsterdam, 2006.
[7] T. Takahashi, K. Takimiya, T. Otsubo, Y. Aso, Org. Lett. 7 (2005) 4313.
[8] T. Takahashi, K. Matsuoka, K. Takimiya, T. Otsubo, Y. Aso, J. Am. Chem. Soc. 27 (2005) 8928.
[9] A. Heeger, S. Kivelson, J.R. Schrieffer, W.P. Su, Rev. Mod. Phys. 60 (1988) 781.
[10] H. Kano, T. Saito, T. Kobayashi, J. Phys. Chem. A 106 (2002) 3445.
[11] K. Nishimura, F.S. Rondonuwu, R. Fujii, J. Akahane, Y. Koyama, T. Kobayashi, Chem. Phys. Lett. 392 (2004) 68.
[12] A. Ozawa, K. Takimiya, T. Otsubo, T. Kobayashi, Chem. Phys. Lett. 409 (2005) 224.
[13] A. Shirakawa, I. Sakane, T. Kobayashi, Opt. Lett. 23 (1998) 1292.
[14] T. Kobayashi, A. Shirakawa, Appl. Phys. B 70 (2000) S239.
[15] A. Baltuska, T. Fuji, T. Kobayashi, Opt. Lett. 27 (2002) 306.
[16] T. Kobayashi, Z. Wang, T. Otsubo, J. Phys. Chem. A, submitted for publication.
[17] S. Adachi, V.M. Kobryanskii, T. Kobayashi, Phys. Rev. Lett. 89 (2002), 027401-1.
[18] T. Kobayashi, H. Wang, Z. Wang, T. Otsubo, J. Chem. Phys. 125 (2006) 044103.
[19] A.R. Bishop, D.K. Campbell, O.S. Lomdahl, B. Horovitz, S.R. Phillpot, Phys. Rev. Lett. 52 (1984) 671.
[20] A.R. Bishop, D.K. Campbell, O.S. Lomdahl, Synth. Met. 9 (1984) 223.
[21] M. Sasai, H. Fukutome, Prog. Theor. Phys. 79 (1988) 61.
[22] A.R. Bishop, D.K. Campbell, P.S. Lomdahl, B. Horovitz, S.R. Phillpot, Phys. Rev. Lett. 52 (1984) 671.
[23] J. Takimoto, M. Sasai, Phys. Rev. B 39 (1989) 8511.
[24] S.R. Phillpot, A.R. Bishop, B. Horovitz, Phys. Rev. B 40 (1989) 1839.
[25] S. Block, H.W. Stritwolf, J. Phys.: Condens. Matter 8 (1996) 889.
[26] P. Maniadis, G.P. Tsironis, A.R. Bishop, A.V. Zolotaryuk, Phys. Rev. E 60 (1999) 7618.
[27] A. Takeuchi, M. Yoshizawa, T. Masuda, T. Higashimura, T. Kobayshi, IEEE J. Quant. Electron. 28 (1992) 2508.
[28] A. Takeuchi, T. Masuda, T. Kobayshi, Phys. Rev. B 52 (1995) 7166.
[29] A. Takeuchi, T. Masuda, T. Kobayshi, J. Chem. Phys. 105 (1996) 2859.
[30] A.T.N. Kumar, F. Rosca, A. Widom, P.M. Champion, J. Chem. Phys. 114 (2001) 701.
[31] A.T.N. Kumar, F. Rosca, A. Widom, P.M. Champion, J. Chem. Phys. 114 (2001) 6795.